

# New constraints on primordial black holes abundance from femtolensing of gamma-ray bursts

A. Barnacka,<sup>1,2,\*</sup> J.-F. Glicenstein,<sup>2,†</sup> and R. Moderski<sup>1</sup>

<sup>1</sup>*Nicolaus Copernicus Astronomical Center, Warszawa, Poland*

<sup>2</sup>*DSM/IRFU/SPP, CEA/Saclay, F-91191 Gif-sur-Yvette, France*

(Dated: November 27, 2024)

The abundance of primordial black holes is currently significantly constrained in a wide range of masses. The weakest limits are established for the small mass objects, where the small intensity of the associated physical phenomenon provides a challenge for current experiments. We used gamma-ray bursts with known redshifts detected by the Fermi Gamma-ray Burst Monitor (GBM) to search for the femtolensing effects caused by compact objects. The lack of femtolensing detection in the GBM data provides new evidence that primordial black holes in the mass range  $5 \times 10^{17} - 10^{20}$  g do not constitute a major fraction of dark matter.

## I. INTRODUCTION

Dark matter is one of the main and most challenging open problems in cosmology or particle physics, and a number of candidates for particle dark matter have been proposed over the years [1]. An alternative idea that the missing matter consists of compact astrophysical objects was first proposed in the 1970s [2–4]. An example of such compact objects are primordial black holes (PBHs) created in the very early Universe from matter density perturbations.

Recent advancements in experimental astrophysics, especially the launch of the FERMI satellite with its unprecedented sensitivity has revived the interest in PBH physics [5, 6]. One of the most promising way to search for PBHs is to look for lensing effects caused by these compact objects. Since the Schwarzschild radius of PBH is comparable to the photon wavelength, the wave nature of electromagnetic radiation has to be taken into account. In such a case, lensing caused by PBHs introduces an interferometry pattern in the energy spectrum of the lensed object [7]. The effect is called ‘femtolensing’ [8] due to very small angular distance between the lensed images. The phenomenon has been a matter of extensive studies in the past [9], but the research was almost entirely theoretical since no case of femtolensing has been detected as yet. Gould [8] first suggested that the femtolensing of gamma-ray bursts (GRBs) at cosmological distances could be used to search for dark matter objects in the mass range  $10^{17} - 10^{20}$  g. Femtolensing could also be a signature of another dark matter candidate: clustered axions [10].

In this paper, we present the results of a femtolensing search performed on the spectra of GRBs with known redshifts detected by the Gamma-ray Burst Monitor (GBM) on board the FERMI satellite. The non observation of femtolensing on these bursts provides new constraints on the PBHs fraction in the mass range

$5 \times 10^{17} - 10^{20}$  g. We describe in details the optical depth derivation based on simulations applied to each burst individually. The sensitivity of the GBM to the femtolensing detection is also calculated.

The paper is organized as follows: in Sec. II the basic equations for femtolensing and the calculation of lensing probability are given. Section III describes the data sample and simulations. In Sec. IV the results are presented, while Sec. V is devoted to discussion and conclusions.

## II. FEMTOLENSING

### A. Magnification and spectral pattern

Consider a lensing event of a GRB by a compact object. The angular diameter distances from the observer to the lens, from the lens to the GRB source and from the observer to the source are  $D_{OL}$ ,  $D_{LS}$ , and  $D_{OS}$ , respectively. Coordinates are taken in the lens plane. The lens, with mass  $M$ , is located at the origin. The source position projected onto the lens plane is given by  $r_S$ , the distance between the lens and true source position. The Einstein radius  $r_E$  is given by

$$r_E^2 = \frac{4GM}{c^2} \frac{D_{OL}D_{LS}}{D_{OL} + D_{LS}} \approx (c \times 0.1 \text{ s})^2 \left( \frac{4\xi - 4}{\xi^2} \right) \left( \frac{D_{OS}}{5 \text{ Gpc}} \right) \left( \frac{M}{10^{19} \text{ g}} \right), \quad (1)$$

where

$$\xi = \frac{D_{OS}}{D_{OL}}. \quad (2)$$

The image positions are given as usual by

$$r_{\pm} = \frac{1}{2}(r_S \pm \sqrt{r_S^2 + 4r_E^2}). \quad (3)$$

The time delay  $\delta t$  between the two images is given by

$$c\delta t = V(r_+; r_S) - V(r_-; r_S), \quad (4)$$

\* e-mail: [abarnack@camk.edu.pl](mailto:abarnack@camk.edu.pl)

† e-mail: [glicens@cea.fr](mailto:glicens@cea.fr)

67 where  $V(r; r_S)$  is the Fermat potential at the position  $r$  96  
68 in the lens plane. One finds:

$$c\delta t = \frac{1}{2} \left( \frac{1}{D_{LS}} + \frac{1}{D_{OL}} \right) (r_+^2 - r_-^2) - \frac{4GM}{c^2} \ln \left( \frac{r_+}{r_-} \right). \quad (5)$$

69 The phase shift between the two images is  $\Delta\phi = E \delta t / \hbar$ ,  
70 where  $E$  is the energy of the photon.

71 In the case of a point source, the amplitude contributed  
72 by the  $r_{\pm}$  images is

$$A_{\pm} \propto \frac{\exp(i\phi_{\pm})}{\sqrt{|1 - \frac{r_E^4}{r_{\pm}^4}|}}. \quad (6)$$

73 The magnification  $A^2$  is obtained by summing the am-  
74 plitudes (6) and squaring, which gives

$$\begin{aligned} |A|^2 &= |A_+ + A_-|^2 = \\ &= \frac{1}{1 - \frac{r_E^4}{r_+^4}} + \frac{1}{1 - \frac{r_E^4}{r_-^4}} + \frac{2 \cos(\Delta\phi)}{\sqrt{|1 - \frac{r_E^4}{r_+^4}|} \sqrt{|1 - \frac{r_E^4}{r_-^4}|}}. \end{aligned} \quad (7)$$

75 The energy dependent magnification produces fringes  
76 in the energy spectrum of the lensed object.

77 In principle, the finite size of the source and the relative  
78 motion of the observer, the lens and the source have to  
79 be taken into account. If the GRB is observed at a time  
80  $t_{expl}$  after the beginning of the burst, its size projected  
81 onto the lens plane is

$$\begin{aligned} s_{GRB} &\approx \frac{D_{OL}}{D_{OS}} \frac{ct_{expl}}{\Gamma} \\ &\approx (c \times 0.005 \text{ s}) \left( \frac{t_{expl}}{1 \text{ s}} \right) \left( \frac{\Gamma}{100} \right)^{-1} \left( \frac{\xi}{2} \right)^{-1}, \end{aligned} \quad (8)$$

82 where  $\Gamma$  is the Lorentz factor of the burst. Note that the  
83 Lorentz factor of GRBs is estimated to be in excess of  
84 100, so that  $s_{GRB}$  given in Eq. (8) is overestimated.

85 The ratio of  $s_{GRB}$  to  $r_E$  is therefore

$$\begin{aligned} \frac{s_{GRB}}{r_E} &\approx 0.05 (\xi - 1)^{-\frac{1}{2}} \left( \frac{t_{expl}}{1 \text{ s}} \right) \left( \frac{\Gamma}{100} \right)^{-1} \\ &\times \left( \frac{D_{OS}}{5 \text{ Gpc}} \right)^{-\frac{1}{2}} \left( \frac{M}{10^{19} \text{ g}} \right)^{-\frac{1}{2}}. \end{aligned} \quad (9)$$

86 Equation (9) shows that the finite size of the GRB can  
87 be in general safely neglected if  $t_{expl} < 10 \text{ s}$ .

88 The Einstein radius crossing time  $t_E$  is given by

$$\begin{aligned} t_E &= \frac{r_E}{v} \\ &\approx 100 \text{ s} \left( \frac{r_E}{c \times 0.1 \text{ s}} \right) \left( \frac{v}{300 \text{ km/s}} \right)^{-1}, \end{aligned} \quad (10)$$

89 where  $v$  is the projected velocity of the source in the lens  
90 plane. Equation (10) shows that  $t_E \gg t_{expl}$  under rea-  
91 sonable assumptions on the velocities. If so, the motion  
92 of the source in the lens plane can also be neglected. In  
93 the analysis of GRB spectra, it is thus assumed that the  
94 point source – point lens assumption is valid and that  
95 the source stays at a fixed position in the lens plane.

## B. Lensing probability

97 The lensing probability of gamma ray burst events is  
98 calculated in two steps. First, the optical depth  $\tau$  for  
99 lensing by compact objects is calculated according to  
100 the formalism of Fukugita et al. [11]. The cosmologi-  
101 cal parameters used in the calculation are: a mean mass  
102 density  $\Omega_M = 0.3$  and a normalized cosmological con-  
103 stant  $\Omega_\Lambda = 0.7$ . The calculations are made for both the  
104 Friedmann-Lematre-Robertson-Walker (FLRW) and the  
105 Dyer-Roeder [12] cosmology. In our sample, the GRB  
106 redshift  $z_s$  is known. The lens redshift  $z_L$  is assumed to  
107 be given by the maximum of the  $d\tau/dz_L(z_S)$  distribu-  
108 tion (see e.g. Fig. 5 of [11]). When  $\tau \ll 1$ , the lensing  
109 probability  $p$  is given by  $p = \tau\sigma$  where  $\sigma$  is the “lensing  
110 cross-section” (see Chap. 11 of [13]).

111 In this paper, the cross-section is defined in the follow-  
112 ing way. Fringes are searched in the spectra of GRBs.  
113 These fringes are detectable only for certain positions  $r_S$   
114 of the source. The exact criteria for detectability will be  
115 given in section III C. The maximum and minimum po-  
116 sition of  $r_S$ , in units of  $r_E$  are noted  $r_{S,min}$  and  $r_{S,max}$ .  
117 They are found by simulation and depend on the GRB  
118 redshift and luminosity. A minimum value of  $r_S$  occurs  
119 because the period of the spectral fringes becomes larger  
120 than the GBM energy range at small  $r_S$ .

121 The femtolensing “cross-section” is simply

$$\sigma = r_{S,max}^2 - r_{S,min}^2 \quad (11)$$

122 The lensing probability does not depend on the indi-  
123 vidual masses of lenses, but only on the density of com-  
124 pact objects  $\Omega_{CO}$ . In the optical depth calculation, an  
125 increase in the mass of the lenses is compensated by a  
126 decrease in the number of scatterers. Therefore, the con-  
127 straints for a given mass depend only on the cross section  
128  $\sigma$ .

## III. DATA ANALYSIS

129  
130 In our analysis, we use a sample of GRBs with known  
131 redshifts. The selection of these bursts is described in  
132 Sec. III A. Then each burst is fitted to a standard spectral  
133 model, as explained in Sec. III B. Finally, the sensitivity  
134 of each burst to femtolensing is studied with simulated  
135 data. The simulation is described in Sec. III C.

### A. Data selection

137 The Gamma-Ray Burst detector (GBM)[14] on-board  
138 the Fermi satellite consists of 12 NaI and 2 BGO scintil-  
139 lators which cover the energy range from 8 keV up to 40  
140 MeV in 128 energy bins. These detectors perform a whole  
141 sky monitoring. In the first two years of operation, GBM  
142 triggered on roughly 500 GRBs. In this paper, only the  
143 bursts with known redshifts have been investigated. The

144 initial sample consisted of 32 bursts taken from Gruber 195  
 145 et al. [15] and 5 additional bursts from the GRB Coordi- 196  
 146 nates Network (GCN) circulars[16]. 197

147 For 17 burst the amount of available data was not suf- 198  
 148 ficient to obtain good quality spectra. The final sample 199  
 149 thus consists of 20 bursts, which are listed in the Tab. I. 200

## 150 B. Data processing and spectral analysis

151 The GBM data are publicly available in the CSPEC 201  
 152 format and were downloaded from the Fermi FSSC web- 202  
 153 site [17]. The CSPEC files contain the counts in 128 203  
 154 energy channels binned in 1.024 s for all detectors. Only 204  
 155 detectors with a minimal signal to noise ratio of 5.5 in 205  
 156 each bin were selected for the analysis.

157 Data were analyzed with the `RMfit` version 33pr7 pro- 206  
 158 gram. The `RMfit` software package was originally devel- 207  
 159 oped for the time-resolved analysis of BATSE GRB data 208  
 160 but has been adapted to GBM and other instruments.

161 For each detector with sufficient data, the background 209  
 162 was subtracted and the counts spectrum of the first ten 210  
 163 seconds of the burst (or less if the burst was shorter) was 211  
 164 extracted. 212

165 The energy spectrum was obtained with a standard 213  
 166 forward-folding algorithm. Several GRB spectral mod- 214  
 167 els such as a broken power law (BKN), Band's model 215  
 168 (BAND) or a smoothly broken power law (SBKN) where 216  
 169 considered. The femtolensing effect was added as a sepa- 217  
 170 rate model. The magnification and the oscillating fridges 218  
 171 where calculated according to Eq. (7), then multiplied 219  
 172 with the BKN or BAND functions. 220

## 173 C. Simulations

174 The detectability of spectral fringes has been studied 221  
 175 with simulated signals. The detectability depends on one 222  
 176 side on the luminosity and the redshift of the bursts, and 223  
 177 on the other side on the detector energy resolution and 224  
 178 the data quality. The sensitivity of the GBM to the lens 225  
 179 mass  $M$  depends strongly also on the energy range and 226  
 180 resolution of the GBM detectors. When small masses 227  
 181 are considered, the pattern of spectral fringes appears 228  
 182 outside of the energy range. The large masses produce 229  
 183 fringes with hardly detectable amplitudes and periods 230  
 184 smaller than the energy bin size. 231

185 Because the data quality and the background are 232  
 186 not easily simulated, the detectability estimation is per- 233  
 187 formed on real data. Namely, GRB events with known 234  
 188 redshift are selected. Since the source redshift is known, 235  
 189 the lens redshift is assumed to be the maximum value 236  
 190 of  $d\tau/dz_L(z_S)$  as explained in Sec. II B. For a given ob- 237  
 191 served GRB, the femtolensing signal depends thus only 238  
 192 on 2 parameters: the lens mass  $M$  and the source posi- 239  
 193 tion in the lens plane  $r_S$ . The data are then processed as 240  
 194 follows: 241

1. The magnification (Eq. 7) as a function of the en-  
 ergy is calculated for the given lens mass  $M$  and  
 position of the source  $r_S$ .
2. This magnification is then convolved with the in-  
 strumental resolution matrix to obtain magnifica-  
 tion factors for each channel of the detector.
3. The spectral signal is extracted from the data by  
 subtracting the background. It is then multiplied  
 by the corrected magnification.
4. The background is added back.

205 The detectability calculation can be illustrated with  
 206 the luminous burst GRB090424592. The spectral data of  
 207 this burst were first fitted with standard spectral models:  
 208 BKN, SBKN and BAND. The GRB090424592 burst is  
 209 best fitted with the BAND model. The fit has  $\chi^2 =$   
 210 78 for 67 degrees of freedom (d.o.f). The BAND model  
 211 has 4 free parameters: the amplitude  $A$ , the low energy  
 212 spectral index  $\alpha$ , the high energy spectral index  $\beta$  and  
 213 the peak energy  $E_{peak}$  [18].

214 The data are then modified by incorporating the spec-  
 215 tral fringe patterns for a range of lens masses  $M$  and  
 216 source positions  $r_S$ . The simulated data and the corre-  
 217 sponding femtolensing fit are presented in Fig. 1. Neither  
 218 BKN nor BAND models are able to fit the simulated data  
 219 (see Fig. 2). The values of  $r_S$  are then changed until the  
 220  $\chi^2$  of the fit obtained is not significantly different from  
 221 the  $\chi^2$  of the unmodified data. More precisely, the  $\chi^2$   
 222 difference  $\Delta\chi^2$  should be distributed in the large sample  
 223 limit as a  $\chi^2$  distribution with 2 degrees of freedom ac-  
 224 cording to Wilk's theorem [19]. The value  $\Delta\chi^2 = 5.99$ ,  
 225 which corresponds to a  $\chi^2$  probability of 5% for 2 d.o.f,  
 226 was taken as the cut value. The effect of changing  $r_S$  on  
 227 the femtolensing model is illustrated on Fig. 3 and 4.

228 In Fig. 5 we show the maximum and minimum de-  
 229 tectable  $r_S$  for different lens masses. The maximum  
 230 difference between  $r_{S,max}$  and  $r_{S,min}$  appears at  $M =$   
 231  $5 \times 10^{18}$  g, which indicates the maximum of femtolensing  
 232 cross-section.

## 233 IV. RESULTS

234 The 20 burst sample from Tab. I have been fitted with  
 235 the standard BKN, BAND and SBKN models. The mod-  
 236 els with the best  $\chi^2$  probability were selected and are  
 237 shown on Tab. I. The bursts are well fitted by these stan-  
 238 dard models, so that there is no evidence for femtolensing  
 239 in the data.

240 As explained in section II B, the lensing probability for  
 241 each burst depends on the lens mass and on the  $r_{S,min}$   
 242 and  $r_{S,max}$  values. Since the sensitivity of GBM to fem-  
 243 to lensing is maximal for lens masses of  $\sim 5 \times 10^{18}$  g  
 244 (see Fig. 5), the values of  $r_{S,min}$  and  $r_{S,max}$  for each  
 245 event were first determined at a mass  $M = 5 \times 10^{18}$  g  
 246 by simulation. As explained in Sec. II B, the value of

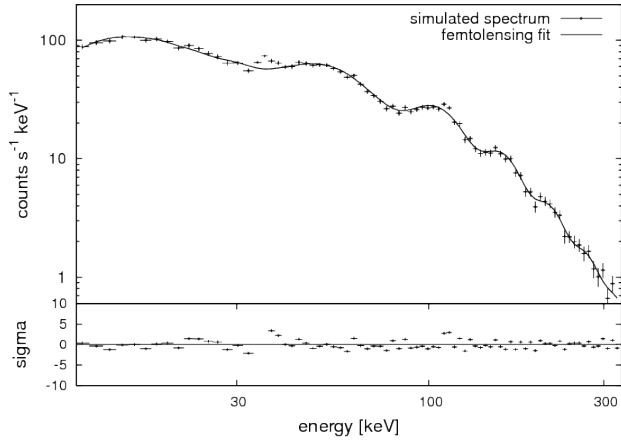


FIG. 1. Simulated spectrum obtained with GRB 090424592. The spectrum was fitted with femtolensing+BAND model. The fit has  $\chi^2 = 92$  for 73 d.o.f. The fit parameters are:  $A = 0.34 \pm 0.02 \text{ ph s}^{-1} \text{ cm}^{-2} \text{ keV}^{-1}$ ,  $E_{peak} = 173 \pm 12 \text{ keV}$ ,  $\alpha = -0.84 \pm 0.03$  and  $\beta = -3.9 \pm 7.5$ . The simulated femtolensing effect is caused by a lens at redshifts  $z_L = 0.256$  and a source at  $z_S = 0.544$ . The simulated mass is  $M = 5 \times 10^{18} \text{ g}$  and the mass reconstructed from the fit is  $5.8 \times 10^{18} \text{ g}$ . The source is simulated at position  $r_S = 2$ . The position reconstructed from the fit is  $r_S = 1.9$ .

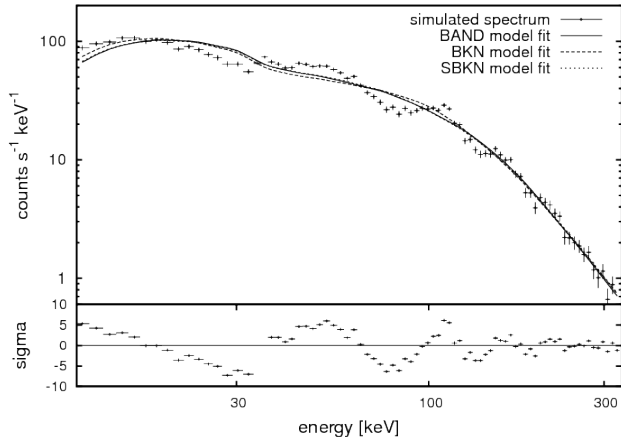


FIG. 2. Simulated femtolensed spectrum fitted with the BAND model. The fit has  $\chi^2 = 810$  for 75 d.o.f. The fit parameters are:  $A = 0.5 \pm 0.03 \text{ ph s}^{-1} \text{ cm}^{-2} \text{ keV}^{-1}$ ,  $E_{peak} = 147 \pm 5 \text{ keV}$ ,  $\alpha = -0.58 \pm 0.03$  and  $\beta = -2.4 \pm 0.1$ . The SBKN model fit is almost indistinguishable from the BKN model fit.

247  $r_{S,min}$  is set by the period of the spectral fringes so that  
 248 it is independent of the burst luminosity. The values of  
 249  $r_{S,max}$  obtained are listed in Tab. I. The lensing prob-  
 250 ability is then calculated for both the FRLW and Dyer  
 251 & Roeder cosmological models using each burst redshift,  
 252 the most probable lens position and the values of  $r_{S,min}$   
 253 and  $r_{S,max}$  for the mass  $M = 5 \times 10^{18} \text{ g}$ . The number  
 254 of expected lensed bursts in the sample is the sum of the  
 255 lensing probabilities. It depends linearly on  $\Omega_{CO}$ .

256 Since no femtolensing is observed, the number of ex-

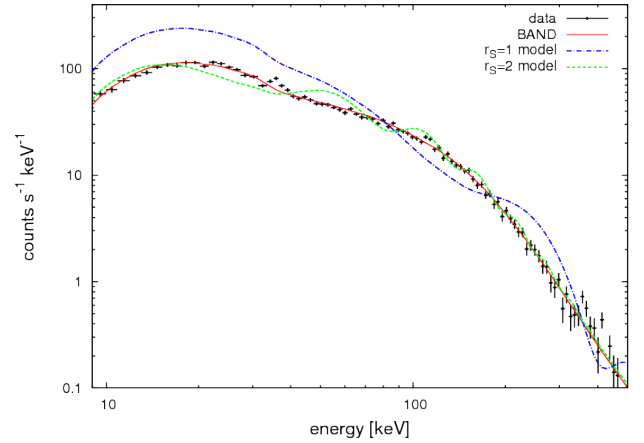


FIG. 3. The spectrum of GRB 090424592 using NaI detector n7, with the BAND and femtolensing fits superimposed. The parameters are  $r_S = 1, 2$ , and lens mass  $5 \times 10^{18} \text{ g}$ . The models are convolved with the response matrix.

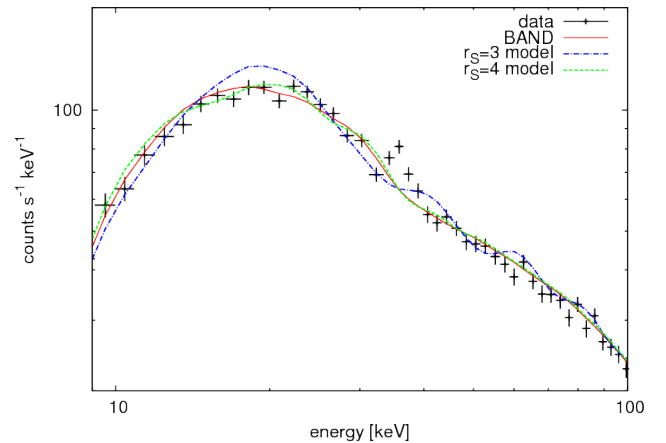


FIG. 4. The spectrum of GRB 090424592 using NaI detector n7. The BAND and femtolensing fits are superimposed. The parameters are  $r_S = 3, 4$ , and lens mass  $5 \times 10^{18} \text{ g}$ . The excess at 33 keV (K-edge) is an instrumental effect seen on many bright bursts.

257 pected events should be less than 3 at 95% confidence  
 258 level (C.L.). The constraints on the density of compact  
 259 objects  $\Omega_{CO}$  is derived to be less than 4% at 95% C.L  
 260 for both cosmological models. The values of the lensing  
 261 probabilities for all the bursts in our sample assuming  
 262 the constrained density of compact objects are shown in  
 263 Tab. I. The limits at other lens masses are obtained by  
 264 normalizing the  $\Omega_{CO}$  at  $M = 5 \times 10^{18} \text{ g}$  by the cross sec-  
 265 tion  $\sigma$ . The cross section is calculated using the Eq. 11  
 266 and the values of  $r_{S,min}$  and  $r_{S,max}$  from Fig. 5. The  
 267 limits on  $\Omega_{CO}$  at 95% C.L. are plotted in Fig. 6.

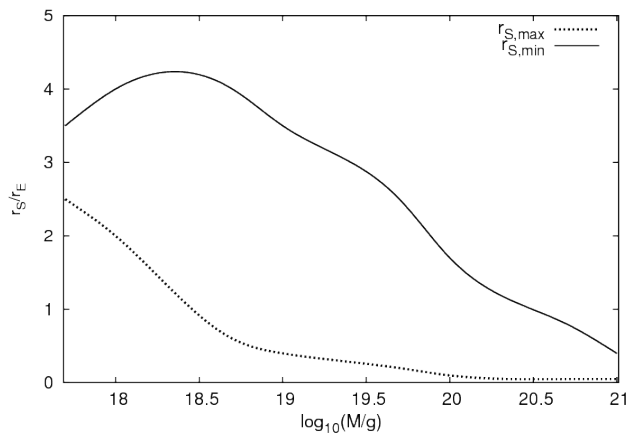


FIG. 5. Minimum and maximum detectable  $r_S/r_E$  as a function of lens mass for GRB 090424592.

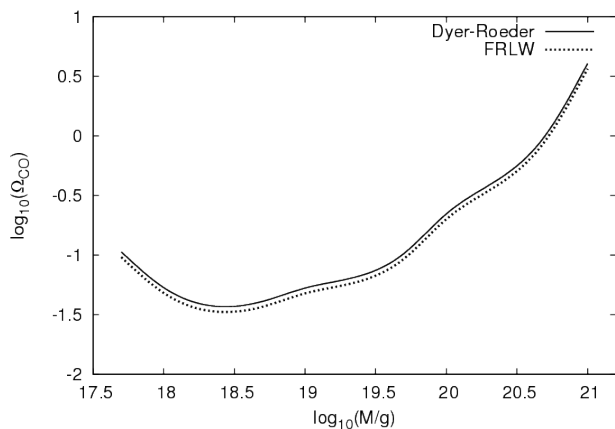


FIG. 6. Constraints on the fraction (or normalized density) of compact objects. The zones above the curves are excluded at the 95% confidence level.

## V. DISCUSSION AND CONCLUSIONS

Cosmological constraints on the PBH abundance are reviewed by Carr et al. [5]. One way to obtain the abun-

dance of PBH is to constrain the density of compact objects  $\Omega_{CO}$ . Note that the limits on the compact object abundance in the  $10^{26} - 10^{34}$  g range obtained with microlensing are at the 1% level.

It is stated in Abramowicz et al. [20] that the mass range  $10^{16}$  g  $< M_{BH} < 10^{26}$  g is virtually unconstrained. Under this range, the  $\Omega_{CO}$  is constrained by PBH evaporation. Above this range, the constraints come from microlensing. The new idea by Griest et al. [6] shows that the microlensing limit could be improved and get constraints down to  $10^{20}$  g with the Kepler satellite observations.

The FERMI satellite was launched three and a half years ago. Since then, almost 1000 of GRB were observed with the GBM detector. In many cases data quality is good enough to reconstruct time-resolved spectra. This unique feature is exploited in our femtolensing search by selecting the first few seconds of a burst in data analysis.

Our limits were obtained by selecting only those bursts with known redshifts in the GBM data. This reduces the data sample from the 500 bursts detected in the first 2 years to only 20. The constraints on  $\Omega_{CO}$  obtained at the 95% C.L. are shown on Fig. 6. These constraints improve the existing constraints by a factor of 4 in the mass range  $5 \times 10^{17} - 10^{20}$  g.

After ten years of operation, the GBM detector should collect over 2500 bursts. Only a few of the bursts, say 100, will have a measured redshift and sufficient spectral coverage. By applying the methods described in this paper, our limits will then improve by a factor of 5 reaching a sensitivity to density of compact objects down to the 1% level.

## ACKNOWLEDGMENTS

Part of this research was supported by the Polish Ministry of Science and Higher Education under grant no. DEC-2011/01/N/ST9/06007 and grant no. ERA-NET-ASPERA/01/10.

- [1] J. L. Feng, *Annual Review of Astronomy and Astrophysics* **48**, 495 (2010), <http://www.annualreviews.org/doi/pdf/10.1146/annurev-astro-082708-101659>.
- [2] B. J. Carr and S. W. Hawking, *Mon. Not. R. Astron. Soc.* **168**, 399 (1974).
- [3] S. W. Hawking, *Nature (London)* **248**, 30 (1974).
- [4] S. Hawking, *Mon. Not. R. Astron. Soc.* **152**, 75 (1971).
- [5] B. J. Carr, K. Kohri, Y. Sendouda, and J. Yokoyama, *Phys. Rev. D* **81**, 104019 (2010), [arXiv:0912.5297](https://arxiv.org/abs/0912.5297) [[astro-ph.CO](https://arxiv.org/abs/0912.5297)].
- [6] K. Griest, M. J. Lehner, A. M. Cieplak, and B. Jain, *Phys. Rev. Lett.* **107**, 231101 (2011), [arXiv:1109.4975](https://arxiv.org/abs/1109.4975) [[astro-ph.CO](https://arxiv.org/abs/1109.4975)].
- [7] A. V. Mandzhos, *Sov. Astron. Lett.* **7**, 213 (1981).
- [8] A. Gould, *Astrophys. J.* **386**, L5 (1992).
- [9] A. Gould, in *Microlensing 2000: A New Era of Microlensing Astrophysics*, Astronomical Society of the Pacific Conference Series, Vol. 239, edited by J. W. Menzies & P. D. Sackett (2001) p. 3, [arXiv:astro-ph/0004042](https://arxiv.org/abs/astro-ph/0004042).
- [10] E. W. Kolb and I. I. Tkachev, *Astrophys. J. Lett.* **460**, L25 (1996), [arXiv:astro-ph/9510043](https://arxiv.org/abs/astro-ph/9510043).
- [11] M. Fukugita, T. Futamase, M. Kasai, and E. L. Turner, *Astrophys. J.* **393**, 3 (1992).
- [12] C. C. Dyer and R. C. Roeder, *Astrophys. J.* **180**, L31 (1973).

- 334 [13] P. Schneider, J. Ehlers, and E. E. Falco, *Gravitational* 360  
 335 *Lenses, XIV, 560 pp. 112 figs.. Springer-Verlag Berlin* 361  
 336 *Heidelberg New York. Also Astronomy and Astrophysics* 362  
 337 *Library* (Springer-Verlag Berlin Heidelberg New York, 363  
 338 1992). 364
- 339 [14] C. Meegan, G. Lichti, P. N. Bhat, E. Bissaldi, 365  
 340 M. S. Briggs, V. Connaughton, R. Diehl, G. Fishman, 366  
 341 J. Greiner, A. S. Hoover, A. J. van der Horst, A. von 367  
 342 Kienlin, R. M. Kippen, C. Kouveliotou, S. McBreen, 368  
 343 W. S. Paciesas, R. Preece, H. Steinle, M. S. Wallace, 369  
 344 R. B. Wilson, and C. Wilson-Hodge, *Astrophys. J.* **702**, 370  
 345 **791** (2009), [arXiv:0908.0450](https://arxiv.org/abs/0908.0450) [astro-ph.IM]. 371
- 346 [15] D. Gruber, J. Greiner, A. von Kienlin, A. Rau, M. S. 372  
 347 Briggs, V. Connaughton, A. Goldstein, A. J. van der 373  
 348 Horst, M. Nardini, P. N. Bhat, E. Bissaldi, J. M. Burgess, 374  
 349 V. L. Chaplin, R. Diehl, G. J. Fishman, G. Fitzpatrick, 375  
 350 S. Foley, M. H. Gibby, M. M. Giles, S. Guiriec, R. M. Kip- 376  
 351 pen, C. Kouveliotou, L. Lin, S. McBreen, C. A. Meegan, 377  
 352 F. Olivares E., W. S. Paciesas, R. D. Preece, D. Tier- 378  
 353 ney, and C. Wilson-Hodge, *Astron. Astrophys.* **531**, 379  
 354 **A20** (2011), [arXiv:1104.5495](https://arxiv.org/abs/1104.5495) [astro-ph.HE]. 380
- 355 [16] [Http://gcn.gsfc.nasa.gov](http://gcn.gsfc.nasa.gov). 381
- 356 [17] [Http://fermi.gsfc.nasa.gov/ssc/](http://fermi.gsfc.nasa.gov/ssc/). 382
- 357 [18] A. Goldstein, J. M. Burgess, R. D. Preece, M. S. 383  
 358 Briggs, S. Guiriec, A. J. van der Horst, V. Connaughton, 384  
 359 C. A. Wilson-Hodge, W. S. Paciesas, C. A. Meegan, 385  
 A. von Kienlin, P. Narayana Bhat, E. Bissaldi, V. Chap-  
 lin, R. Diehl, G. J. Fishman, G. Fitzpatrick, S. Foley,  
 M. Gibby, M. Giles, J. Greiner, D. Gruber, R. M. Kip-  
 pen, C. Kouveliotou, S. McBreen, S. McGlynn, A. Rau,  
 and D. Tierney, ArXiv e-prints (2012), [arXiv:1201.2981](https://arxiv.org/abs/1201.2981)  
 [astro-ph.HE].
- [19] J. R. Mattox, D. L. Bertsch, J. Chiang, B. L. Dingus,  
 S. W. Digel, J. A. Esposito, J. M. Fierro, R. C. Hart-  
 man, S. D. Hunter, G. Kanbach, D. A. Kniffen, Y. C.  
 Lin, D. J. Macomb, H. A. Mayer-Hasselwander, P. F.  
 Michelson, C. von Montigny, R. Mukherjee, P. L. Nolan,  
 P. V. Ramanamurthy, E. Schneid, P. Sreekumar, D. J.  
 Thompson, and T. D. Willis, *Astrophys. J.* **461**, **396**  
 (1996).
- [20] M. A. Abramowicz, J. K. Becker, P. L. Biermann,  
 A. Garzilli, F. Johansson, and L. Qian, *Astrophys. J.*  
**705**, **659** (2009), [arXiv:0810.3140](https://arxiv.org/abs/0810.3140).
- [21] G. F. Marani, R. J. Nemiroff, J. P. Norris, K. Hurley,  
 and J. T. Bonnell, *Astrophys. J. Lett.* **512**, **L13** (1999),  
[arXiv:astro-ph/9810391](https://arxiv.org/abs/astro-ph/9810391).
- [22] M. S. Briggs, D. L. Band, R. D. Preece, G. N. Pendle-  
 ton, W. S. Paciesas, and J. L. Matteson, in *Gamma-Ray*  
*Bursts, 4th Hunstville Symposium*, American Institute of  
 Physics Conference Series, Vol. 428, edited by C. A. Mee-  
 gan, R. D. Preece, & T. M. Koshut (1998) pp. 299–303,  
[arXiv:astro-ph/9712096](https://arxiv.org/abs/astro-ph/9712096).

TABLE I. The sample of 20 GBM GRBs used in the analysis.

Name	$z_S$	Fit to simulated data						Lensing Probability	
		Fit to the data <sup>a</sup>		Model	Femtolensing	$r_{S,max}$	$z_L$	FRLW <sup>b</sup>	Dyer-Roeder <sup>c</sup>
		Model	$\chi^2/d.o.f$	$\chi^2/d.o.f$	$\chi^2/d.o.f$				
GBM 080804972	2.2045	BAND	68/74	116/63	65/61	2	0.770	0.110	0.112
GBM 080916009C	4.3500	BKN	68/75	91/86	78/84	3	1.087	0.580	0.539
GBM 080916406A	0.6890	BKN	58/57	122/87	110/85	3	0.324	0.036	0.040
GBM 081121858	2.5120	BKN	39/49	52/49	42/47	3	0.829	0.296	0.298
GRB 081222204	2.7000	BKN	73/66	82/62	63/60	3	0.859	0.326	0.325
GRB 090102122	1.5470	BAND	81/85	103/85	93/83	3	0.603	0.146	0.154
GRB 090323002	3.5700	BAND	77/77	121/64	90/62	2	0.964	0.206	0.197
GRB 090328401	0.7360	BKN	105/70	123/70	103/68	2	0.346	0.018	0.020
GRB 090424592	0.5440	BAND	78/67	115/75	97/73	4	0.256	0.042	0.046
GRB 090510016	0.9030	BKN	62/66	173/98	158/96	1.5	0.406	0.015	0.016
GRB 090618353	0.5400	BAND	59/72	79.5/72	66/70	3	0.254	0.023	0.025
GRB 090926181	2.1062	BAND	87/81	105/81	93/79	4	0.737	0.413	0.423
GRB 091003191	0.8969	BKN	93/94	105/94	94/92	3	0.400	0.059	0.064
GRB 091020900	1.7100	BKN	74/69	116/69	90/67	2.5	0.667	0.119	0.124
GRB 091127976	0.4900	BAND	78/74	84/74	76/72	4	0.240	0.034	0.037
GRB 091208410	1.0630	BAND	55/55	115/59	56/57	2.5	0.457	0.055	0.059
GRB 100414097	1.3680	BKN	65/61	97.5/68	86/66	2.5	0.560	0.084	0.089
GRB 100814160A	1.4400	BKN	42/40	138/42	128/40	2	0.590	0.058	0.061
GRB 100816009	0.8049	BKN	73/52	95/50	66/48	2.5	0.360	0.034	0.037
GRB 110731465	2.8300	SBKN	72/64	125/64	97/62	3	0.877	0.347	0.344

<sup>a</sup> Fit has been performed using only the photons arrived in less than 10s from the beginning of the burst.<sup>b</sup> for assumed  $\Omega_{CO} = 0.037$ <sup>c</sup> for assumed  $\Omega_{CO} = 0.041$